Environmental Science: Atmospheres

ROYAL SOCIETY OF CHEMISTRY

PAPER

View Article Online
View Journal | View Issue

Cite this: *Environ. Sci.: Atmos.*, 2023, **3**, 568

Wintertime spatial patterns of particulate matter in Fairbanks, AK during ALPACA 2022†

Ellis S. Robinson, *[a] Meeta Cesler-Maloney,[bc] Xinxiu Tan,[a] Jingqiu Mao,[bc] William Simpson[bc] and Peter F. DeCarlo *[a]

Fairbanks-North Star Borough (FNSB), Alaska perennially experiences some of the worst wintertime air quality in the United States. FNSB was designated as a "serious" nonattainment area by the U.S. Environmental Protection Agency in 2017 for excessive fine particulate matter ($PM_{2.5}$) concentrations. The ALPACA (Alaskan Layered Pollution And Chemical Analysis) field campaign was established to understand the sources of air pollution, pollutant transformations, and the meteorological conditions contributing to FNSB's air quality problem. We performed on-road mobile sampling during ALPACA to identify and understand the spatial patterns of PM across the study domain, which contained multiple stationary field sites and regulatory measurement sites. Our measurements demonstrate the following: (1) both the between-neighborhood and within-neighborhood variations in $PM_{2.5}$ concentrations and composition are large (>10 μg m^{-3}). (2) Spatial variations of PM in Fairbanks are tightly connected to meteorological conditions; dramatic between-neighborhood differences exist during strong temperature inversion conditions, but are significantly reduced during weaker temperature inversions, where atmospheric conditions are more well mixed. (3) During strong inversion conditions, total $PM_{2.5}$ and black carbon (BC) are tightly spatially correlated and have high absorption Ångstrom exponent values (AAE > 1.4), but are relatively uncorrelated during weak inversion conditions and have lower AAE. (4) $PM_{2.5}$, BC, and total particle number (PN) concentrations decreased with increasing elevation, with the fall-off being more dramatic during strong temperature inversion conditions. (5) Mobile sampling reveals important air pollutant concentration differences between the multiple fixed sites of the ALPACA study, and demonstrates the utility of adding mobile sampling for understanding the spatial context of large urban air quality field campaigns. These results are important for understanding both the PM exposure for residents of FNSB and the spatial context of the ALPACA study.

Received 24th October 2022
Accepted 13th January 2023

DOI: 10.1039/d2ea00140c

rsc.li/esatmospheres

Environmental significance

Our work aims to understand the ambient spatial patterns of key particulate pollutants—$PM_{2.5}$, black carbon, and particle number—in a high latitude Arctic city, Fairbanks, AK. Fairbanks perennially has some of the worst wintertime air quality in the US. Using a mobile sampling platform, we show that residential neighborhoods are air pollutant hotspots and that residential biomass-burning is the emissions source driving these hotspots. Importantly, almost all of the stark spatial variability is significantly reduced when the surface-based temperature inversion is weak compared to when it is strong, emphasizing the key role that meteorology plays in determining air quality in Fairbanks and other Arctic cities. These findings extend the literature of mobile air pollution measurements and urban air quality to high-latitude areas. They provide context to conversations between the Fairbanks community and local decision-makers.

1 Introduction

Fairbanks, Alaska is a small city with a large wintertime air quality problem. Fairbanks (pop. approximately 33 000, 2020 Census) is situated in the larger Fairbanks-North Star Borough (FNSB, pop. approximately 96 000, 2020 U.S. Census). FNSB regularly experiences fine particulate matter ($PM_{2.5}$) pollution episodes in the winter that exceed the U.S. Environmental Protection Agency (EPA) 24 h regulatory limit (35 μg m^{-3}) for weeks-long stretches.[1] While year-over-year concentrations of $PM_{2.5}$ in FNSB have been declining over the past decade,[2] FNSB was labeled a "serious non-attainment area" by the EPA in 2017 [3] and is the highest-ranking city in the American Lung Association's most recent State of the Air report for metropolitan areas with the worst short-term PM pollution.[4]

The air quality problem in FNSB is caused both by strong emissions from local sources and poor dispersion, each of which

[a]*Environmental Health & Engineering, Johns Hopkins University, Baltimore, Maryland, USA. E-mail: shipleyrobinson@gmail.com; pdecarl1@jhu.edu*
[b]*Chemistry & Biochemistry, University of Alaska Fairbanks, Fairbanks, Alaska, USA*
[c]*Geophysical Institute, University of Alaska Fairbanks, Fairbanks, Alaska, USA*

† Electronic supplementary information (ESI) available. See DOI: https://doi.org/10.1039/d2ea00140c

are exacerbated by the extreme cold.[2] The major emissions sources in the region are home heating, power generation, and transportation.[5,6] Domestic heating typically comes from burning fuel oil or biomass (either cordwood or pellets), with a small amount of heating coming from electric and natural gas.[7] While some of the more urban sectors of both Fairbanks and North Pole are served by natural gas, natural gas has been less commonly used for heating than oil or wood, due both to historical unavailability and consumer attitudes.[7] Previous work has used long-term source apportionment to better understand PM pollution in Fairbanks,[8–11] and while these studies represent a range of estimates of the woodsmoke fraction to total $PM_{2.5}$ (40–80%), they generally agree that it is the single largest source in the area during wintertime. Other PM types, including secondary particulate pollution (*e.g.* hydroxymethanesulfonate, HMS[12]) have been shown to be important as well, though the spatial patterns of PM components or their gas-phase precursors are unknown.

Poor atmospheric dispersion, due to both meteorological conditions and local topography, exacerbates the aforementioned emissions issues. In the depths of winter, FNSB only receives a few hours of daylight at low solar elevation, and the area has a relatively high albedo due to complete snow coverage.[13] This lack of solar heating means vertical convective mixing can be absent for long stretches, allowing very strong temperature inversions to develop. These surface based inversions (SBIs) can exceed 0.5 °C m^{-1} in the lowest 10 m above ground level.[14,15] Additionally, Fairbanks is situated in the Tanana River Valley, and the surrounding hills and mountains protect the area from winds that could aid in dispersion. With little shear winds or vertical convection to disperse pollutants, and a very shallow boundary layer, local emissions, which are strongest during extreme cold, often have nowhere to go.

We hypothesized that the typical spatial patterns of air pollution elucidated by previous studies from mid-latitude urban areas may be different in FNSB. For example, a substantial fraction of the air pollutant land-use regression literature relies on data collected from mobile platforms, but rarely includes meteorological variables for predicting pollutant concentration surfaces. However, previous work in Fairbanks has shown that cold temperatures and SBI dramatically influence ground-level air pollution measurements.[15,16] Similarly, the spatial scales of air pollution-how pollutant concentration decays with radial distance from sources-may be quite different with strong SBI conditions and a very low boundary height. Lastly, both the source mix in Fairbanks (heavy reliance on heating oil and wood-burning) and the high per-capita demand for heating is simply different from most locations where mobile air quality sampling has informed our understanding of pollutant spatial patterns.

The ALPACA field campaign aims to better understand the above interplay between sources and meteorology, as well as the chemical transformations of air pollutants in extreme cold and dark environments.[2] The campaign will shed more light on the similarities of air quality processes in Fairbanks to other mid-latitude cities, but also what aspects of air quality, due either to sources or meteorology (or both), are uniquely important for high-latitude urban areas. Insights will not only be relevant in Fairbanks, but also more broadly to other high-latitude urban areas, especially as Arctic and sub-Arctic urban populations are expected to grow in coming decades.[17]

We performed mobile sampling during ALPACA in order to understand how particulate pollutant concentrations and exposures may vary across the city of Fairbanks. We also sought to establish the spatial context of the ALPACA project itself, in order to understand how each field site may be impacted by local sources differently for the purposes of intercomparison. Fig. 1 shows the location of the ALPACA field sites and Alaska Department of Environmental Conservation (ADEC) monitoring sites along the mobile sampling route.

Herein, we present mobile-based measurements of $PM_{2.5}$, particle number (PN), and black carbon (BC). We find strong spatial pollution gradients both between neighborhoods and within neighborhoods, largely during periods with strong SBI, which emphasizes the importance of meteorological conditions in interpreting results from mobile sampling. Our results can inform the community of Fairbanks, the mobile air pollution sampling literature, and the high-latitude urban air pollution literature.

2 Methods

2.1 Experimental design

Our sampling plan focused on "temporal depth" instead of "spatial breadth." We repeatedly visited a smaller number of

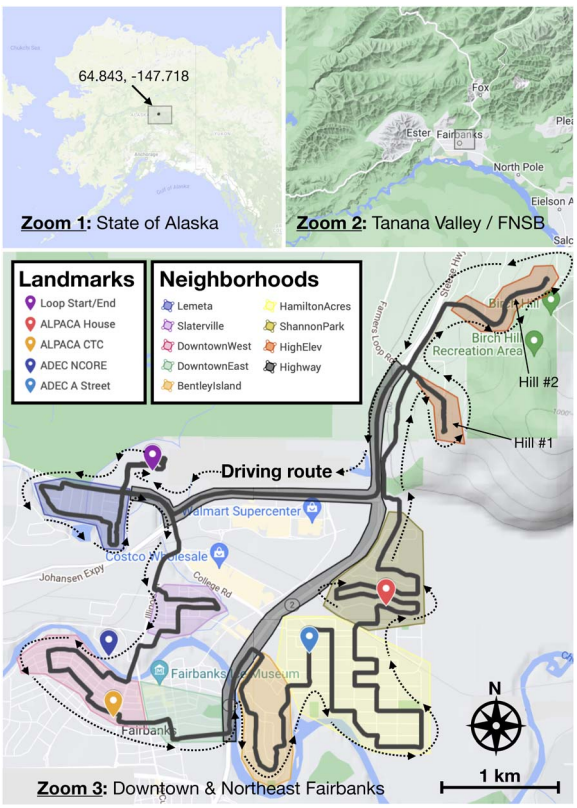

Fig. 1 Map of study domain at different levels of zoom to illustrate the position of our driving route in the world, the Tanana River Valley, and FNSB. Map of highest zoom shows the driving route, neighborhood boundaries, and fixed-site locations.

locations rather than a larger, potentially more varied sampling domain where we would visit each location fewer times. We drove the sampling route 29 times over 24 different days between January 17, 2022 and February 27, 2022, though driving was clustered during two intensive periods: mid-late January at the beginning of ALPACA, and mid-late February at the end of the campaign. The details of all drives are listed in Table S1 and Fig. S1† shows a time series of stationary $PM_{2.5}$ measurements made at the ALPACA house site, with mobile sampling periods highlighted in red. We spread sampling periods across time of day (as shown in Fig. S2c†) and over weekdays and weekends, in an effort not to over-represent a certain portion of the diurnal or weekly pattern for any of the pollutants measured.

The sampling route was optimized according to the following criteria: (1) route contained multiple residential neighborhoods, (2) route covered a range of land-use types (*e.g.* busy and non-busy roads, residential and commercial, high elevation and low elevation), and (3) route passed by as many of the stationary field sites as possible, to allow for intercomparison. Lastly, we aimed to accomplish the above objectives as best as possible within a 1.5 hour timeframe for each drive, due to time constraints imposed by the larger ALPACA project. Additionally, because of how strongly meteorological conditions in Fairbanks influence pollutant concentrations, as shown by Cesler-Maloney *et al.*,[15] we sampled across a range of SBI strengths.

We aimed to visit each location in the domain at least 10 different times within each of two inversion strength categories ("strong inversion" and "weak inversion" conditions, defined below), knowing that air quality patterns may be quite different across SBI strength. Apte *et al.*[18] showed that 10 or more unique mobile lab visits were sufficient to characterize representative concentrations of NO, NO_2, and BC in space across Oakland, CA. Without knowing *a priori* how many repeated visits were needed for this domain and the pollutants we measured, we used this rough guide of a 10+ visits thresholds within each SBI category to plan our sampling. We discuss how representative our sampling was further in Results.

2.2 Instrumentation and measurements

2.2.1 $PM_{2.5}$ (DustTrak). We measured PM_1/$PM_{2.5}$/PM_4/PM_{10}/total suspended particle (TSP) mass using a DustTrak (DustTrak DRX Aerosol Monitor 8533, TSI Inc., USA). The DustTrak was operated on battery-power and has a sampling rate of 1 Hz. We operated the instrument without any impactor, in order to measure all size fractions, though our measurements indicated that the very large majority (97%) of all DustTrak-measured PM was 2.5 μm or less (see Fig. S3† for details), and so we only report $PM_{2.5}$ here.

We applied the TSI-suggested 0.38 correction factor for ambient measurements to the default DustTrak settings, which are calibrated using Arizona Test Dust, which has a much higher density (2.65 g cm^{-3}) than PM dominated by organic aerosol (typical density of roughly 1–1.5 g cm^{-3}). It should be noted that we do not have co-located gravimetric measurements of $PM_{2.5}$ to compare against to definitively test this correction factor. The DustTrak "zero calibration" procedure was performed using a HEPA filter prior to departing for each sampling drive. We sampled through a HEPA filter at the start and end of each drive, in order to do a zero-check of each instrument and to "mark" the time series data of each drive with start and stop periods.

All instruments relying on light scattering (like the DustTrak) have a lower size limit for particle detection due to inherent limitations of measuring scattered light from small particles, though this size cutoff can vary considerably across instruments due to detector quality, light source wavelength and intensity, and other factors.[19] The manufacturer-stated lower particle-diameter cut-off is 100 nm, and so the $PM_{2.5}$ measurements we report here only account for particles larger than this lower limit. Approximately 73% of aerosol volume measured during ALPACA is above 100 nm according to stationary SMPS measurements (see Fig. S4† for details), and thus roughly 27% of the aerosol volume is not measured by the DustTrak instrument. Thus, any spatial patterns we report here are biased towards >100 nm particles, and while that does represent the majority of the ambient aerosol during our mobile sampling periods, there is possibly a class (or multiple) of aerosol types whose spatial patterns we do not fully capture.

2.2.2 Particle number (MAGIC CPC). Total particle number (PN) was measured with a water-based condensation particle counter (MAGIC 210 CPC, Aerosol Devices Inc., USA). The instrument was operated on battery-power and has a sampling rate of 1 Hz. The MAGIC (Moderated Aerosol Growth with Internal water Cycling) CPC uses condensational growth to optically count particles as small as 5 nm. There is a 2.5 μm impactor in the inlet of the instrument, limiting the upper particle size that the instrument can detect.[20] The upper detection limit of PN concentration in the instrument is 10^6 cm^{-3}.

2.2.3 Light-absorbing PM (microAeth). We measured light-absorbing PM mass using a 5-wavelength micro-aethalometer (microAeth MA350, AethLabs, USA). Wavelengths for the instrument are 375 nm, 470 nm, 528 nm, 625 nm, and 880 nm. The microAeth was operated with a 1 Hz sampling rate and was operated on battery-power. We interpret the concentration of light-absorbing PM from the 880 nm measurement as BC. Due to instrument noise, we applied median smoothing to the microAeth data using a 30 second rolling window.

Absorption Ångstrom exponent (AAE) is a physical parameter indicating the wavelength-dependence of aerosol light absorption. AAE can inform PM source apportionment, given characteristic AAE values of different aerosol types, such as traffic and biomass-burning PM. Many previous studies have examined AAE of different aerosol types,[21,22] and identified how physical and chemical processes can influence AAE (*e.g.* lensing effect through particle coatings, chemical aging, *etc.*).[23,24] It is not a sharp tool alone for identifying *e.g.* the presence of brown carbon (BrC), as no perfect AAE threshold(s) exist for definitive source apportionment. However, typically, pure BC particles have relatively weak spectral dependence of light-absorption, and so have AAE close to 1, while AAE values well-above 1 generally indicate the additional presence of non-BC light

absorbing components, such as BrC.[22] Traffic-related PM tends to have AAE around 1,[22] while AAE from biomass-burning can be quite variable,[21] but tends to be well-above 1. We do not use our AAE measurements to perform quantitative source apportionment here, nor try to quantify the concentration of BrC; instead, we present spatial patterns of AAE and refer to it as a rough proxy measurement that is suggestive of different PM sources. Based on Zhang *et al.*,[25] who showed that AAE from BC can range from 0.7–1.4 depending on the presence of non-absorbing coatings, we use AAE > 1.4 as a rough delineation above which there is likely a contribution of BrC to the light-absorbing PM fraction.

We calculated AAE using the following equation:

$$\mathrm{AAE} = -\frac{\ln\left(\frac{b_{880}}{b_{375}}\right)}{\ln\left(\frac{\lambda_{880}}{\lambda_{375}}\right)} \quad (1)$$

where b_i is the optical absorption coefficients at a given wavelength, λ_i. We use the 880 nm and 375 nm to calculate AAE because these wavelengths span the full range over which that the microAeth measures attenuation.

2.2.4 Inlet and flows. Our sampling inlet was positioned roughly 0.5 m above the roof of a standard-size sport utility vehicle (roughly 2 m above ground level), with the mouth of the inlet pointed in the direction of travel in order to minimize loss of large particles. A cross-country skiing pole (Swix, Quantum 4) was used to stabilize the particle sampling line exterior to the vehicle. Almost all sampling tubing was conductive silicone (4.75 mm ID), with stainless steel "Y" fittings (4.70 mm ID; Model 1100, Brechtel, USA) used to split the aerosol flow from the main sampling line to each instrument's inlet in order to minimize particle losses. Sampling tubing between the main sampling line and the microAeth was 2 mm ID conductive silicone. A schematic of the mobile sampling platform, including inlet lengths and flows, is shown in Fig. S5.†

The sampling flows for the DustTrak, MAGIC CPC, and microAeth are 1, 0.3, and 0.1 liters per minute (LPM), respectively. We calculate the total residence time for particles in the sampling lines for each instrument above to be 0.4, 1.1, and 1.6 seconds, respectively. These calculations account for both the shared flows in common lines and the individual sampling line of each instrument. Because we joined measurements by timestamps rounded to the nearest second, we also rounded the total residence time for each instrument to the nearest second (*e.g.* 0, 1, and 2 second, respectively, for the DustTrak, microAeth, and MAGIC CPC), and then shifted each measurement accordingly. Our conclusions were not sensitive to whether or not we applied this temporal shift.

2.2.5 GPS. We used a cycling computer (ELEMNT BOLT, Wahoo Fitness, USA) recording position and elevation at 1 Hz intervals. We were unable to find a stated accuracy from the manufacturer, but never had any noticeable GPS "wanderings," and so qualitatively assume that the positional accuracy is likely on the same order as the width of a typical road in Fairbanks (roughly 6 m), which is substantially less than the length-scale of the spatial aggregation we perform in our data analysis. All GPS measurements were uploaded to Strava (**https://www.strava.com**), and then downloaded as data frames through the Strava API using the *rStrava* library in R.

2.2.6 Vertical temperature measurements. Temperature measurements from the downtown field site used to characterize inversions were made using custom sensors described fully in Cesler-Maloney *et al.*[15] In short, temperature probes were placed within PVC pipes serving as a radiation shield, and had fans pulling air over them to provide ventilation and a constant stream of ambient air. The data was logged on two data loggers (CR1000X, Campbell Scientific, USA) at 1 min time resolution.

We measured temperatures both near ground level (3 m) and atop the roof of a three-story public building (25 m) at 5 minute resolution. The average temperature difference between 25 m and 3 m ($\Delta T = T_{25\ \mathrm{m}} - T_{3\ \mathrm{m}}$) over the 3 hours prior to the start of the drive is the measure we use to characterize the SBI strength for each drive.

2.2.7 Instrument co-location. We also performed side-by-side co-location with other particle instruments at the ALPACA house field site, in an effort to double-check the accuracy of the mobile instrument suite to measure ambient aerosols in Fairbanks. We co-located instruments during portions of Feb. 4–7, Feb. 15–16, and Feb. 24, 2022. These intercomparisons were not used to correct any of the mobile data, but solely to validate the accuracy of the mobile instrument suite compared to higher-grade stationary instruments. ALPACA house measurements included: an Aerosol Mass Spectrometer (AMS, Aerodyne Research, Inc., USA) for measuring non-refractory sub-micron PM (NR-PM_1), an aethalometer (AE-33, Magee Scientific, USA) for BC, and a Scanning Mobility Particle Sizer (SMPS, TSI, Inc., USA) for PN. SMPS scans were integrated across all size bins to provide total PN.

During co-location periods, the mobile instrumentation suite was connected to the particle sampling manifold *via* a "Y" split fitting. The ALPACA house field site was designed to better understand outdoor–indoor air pollutant transformations and concentrations in Fairbanks, and employed a sampling strategy where the sampling line switched back-and-forth on a 10 minute schedule between sampling outdoor and indoor air through an automated valve system. We performed the co-located sampling between the two main periods of driving in the campaign, and each co-location lasted longer than 10 hours. The long duration of the co-locations and the indoor–outdoor sampling switching, where indoor PM concentrations are typically substantially lower than outdoor concentrations, provided a large dynamic concentration range for the intercomparison for each pollutant. There were no indoor perturbations (*e.g.* food cooking, pellet stove burning) included in the intercomparison periods.

Co-location data was cleaned in the following ways to allow for proper intercomparison: in the cases of AMS (Aerosol Mass Spectrometer, NR-PM_1) and SMPS (Scanning Mobility Particle Sizer, PN), which have long integration times relative to the 1 Hz mobile instruments, we averaged mobile-instrument data across the duration of each *e.g.* AMS scan. AMS and SMPS scans that spanned a change in valve-state from outdoor-to-indoor (or

vice versa) were removed. Because the AMS only measures non-refractory sub-micron PM, we add BC measured by the AE-33 to get a total PM_1 measurement comparable to the DustTrak, which should measure both non-refractory and BC species for particles above 100 nm.

2.3 Data analysis

All 1 Hz mobile measurements were rounded to the nearest second, and then joined by timestamp. All spatial data analysis was performed using the *sf* library in R. Other R libraries used in our data analysis and visualization include *lubridate*, *tidyverse*, *googlesheets4*, *wesanderson*, and *openair*. All data analysis was performed using R software.

2.3.1 Spatial aggregations. Spatial aggregation is an important part of any mobile air quality study. We aggregate pollutant data for each drive into 50 m grid cells. Given a typical vehicle speed of 15 miles per hour (7 m s^{-1}), there are roughly seven 1 Hz measurements in each cell per drive, though this number can be quite variable due to uneven vehicle speeds, and, in the extreme case, stopping. Thus, spatial aggregation at 50 m helps reduce bias introduced by non-uniform speeds and we use the mean of all measurements in each cell for each drive (the "drive-mean") as our concentration values at high spatial resolution. Spatially-resolved "representative" pollutant concentrations are the mean of all drive-mean concentrations for each grid cell. Any grid cell concentration reported in this manuscript meets a requirement of having a minimum of 10 unique visits, including within each inversion category. Almost all grid cells met the 10+ visit threshold, though due either to instrument downtime or short amendments of the route due to road closures, *etc.* some grid cells did not, in which case they are not included as representative concentrations in any of the proceeding maps or analysis.

We also performed "neighborhood"-level spatial aggregation to assess the between-neighborhood and within-neighborhood spatial concentration differences for the parts of our sampling domain where people live. Neighborhoods were drawn with a colloquial sense of distinct residential housing areas (*e.g.* a group of blocks within the same enclave not separated by major roads or land features). The neighborhood units are also roughly equal in size (roughly 0.5 km^2), and contain roughly similar numbers of 50 m grid cells. They are named according to local nomenclature (see Fig. 1). These boundaries and names are useful in terms of categorizing different residential areas, but do not represent official municipal boundaries.

We assessed in post-processing whether self-sampling of our vehicle exhaust impacted or biases our dataset, and determined that it did not. As such, we have not filtered our dataset for stops or accelerations.

2.3.2 Spatial representativeness. We assess the representativeness of our data following a similar approach to Targino *et al.*[26] Without separating into inversion categories, we perform the following analysis on our full dataset: for each pollutant within each grid cell, we calculate a cumulative mean value by randomly sampling (without replacement) the visits we made. We perform this procedure 100 times, and use the spread (as indicated by the IQR) in the calculated cumulative mean to assess how confident we are in the grid cell mean for a given number of visits. Finally, we look for the number of visits that are required for the metric of the IQR of cumulative means divided by the overall mean (IQR/mean) to fall below 20%. Unlike Targino *et al.*, we are using the cumulative mean here because we are reporting mean values for each grid cell. These analysis steps are illustrated graphically in Fig. S6.†

In addition, we examined our confidence in being able to distinguish mean concentrations (for each pollutant, for each grid cell) between the two inversion conditions. Similar to above, we perform the same sampling approach by calculating the cumulative mean value for a given number of visits, but now separating our dataset into the two inversion conditions. We then compare the 25th percentile of cumulative means at 10 visits in the strong inversion category to the 75th percentile of cumulative means at 10 visits in the weak inversion category. In other words, we compare the lower bound of our confidence in the higher-value mean to the upper bound of confidence in the lower-value mean. For all but a single grid cell in our dataset, the overall grid cell mean for the strong inversion category was larger than for the weak inversion category. If the difference in the 25th percentile (for strong) and the 75th percentile (for weak) were small (or negative), it would indicate too much overlap in spread of cumulative mean values to reasonably be able to detect differences between the two conditions. These analysis steps are illustrated graphically in Fig. S7.†

3 Results

3.1 Spatial representativeness

Based on our sub-sampling analysis, we are confident that our measurements provide a robust representation across space for pollutant concentrations in Fairbanks for the months of January and February. Fig. S6c† shows a histogram illustrating the distribution in the number of repeated visits it took for grid cells to converge to towards their mean $PM_{2.5}$ concentrations. All grid cells converged within 22 visits (median of 15 visits), which is less than the 29 total visits in our dataset. Results were similar for both BC and PN as well.

Additionally, we assessed whether or not we could be confident in distinguishing between mean values at each location for each of the two inversion conditions. Fig. S7b† shows the distribution of the difference between the lower and upper bounds of our confidence in the mean value ("$\Delta PM_{2.5}$") calculated for 10 visits between the strong and weak inversion condition, respectively. The large majority of grid cells had positive $\Delta PM_{2.5}$ values, indicating that the uncertainty in the grid cell mean value at 10 visits was less than the difference between the overall grid cell means, and thus supports our ability to ascribe real concentration differences between the two conditions. Only four of the 500 total grid cells had negative $\Delta PM_{2.5}$ values, which indicates an overlap in the confidence interval and thus an inability to distinguish a difference between the two conditions. Based on this analysis, we are confident in both the spatial representativeness of this dataset

and our ability to distinguish concentrations between the two inversion conditions across most of the domain.

3.2 Pollutant spatial variability

Concentration maps for the three pollutants are shown in Fig. 2. Here we present mean grid cell concentrations for all locations with 10+ visits, though most had far more given the 29 total drives of the campaign. Despite the relatively small area (10 km^2) of the sampling domain, we observe substantial spatial variations in concentrations for each pollutant. The maps reveal a mix of both small- and large-scale areas of high PM levels, or "hotspots." For example, much of the south-central portion of the map—containing parts of Downtown East, Bentley Island, and Hamilton Acres neighborhoods—shows high $PM_{2.5}$ concentrations spread out over an area on the same order of size as the neighborhoods. There are multiple small-scale hotspots within neighborhoods across the domain as well, *e.g.* the southern tip of the Lemeta neighborhood, various locations in Hamilton Acres, and parts of Downtown West. The mix of neighborhood- and sub neighborhood-scale pollution gradients implies variable source strengths both between and within neighborhoods in Fairbanks.

We summarize these neighborhood- and sub-neighborhood-level gradients in $PM_{2.5}$, PN, and BC concentrations in Fig. 3 using boxplots of the grid cell mean concentrations from the maps in Fig. 2. We also plot the distribution of grid cell mean AAE values. The neighborhood ordering on the *x*-axis is by increasing concentration of $PM_{2.5}$. Excluding the HighElev and Highway aggregations, Shannon Park is the residential neighborhood with the lowest median in grid cell $PM_{2.5}$ concentration (14.5 μg m^{-3}) and Bentley Island is the highest (22.5 μg m^{-3}). This spread in $PM_{2.5}$ concentrations across neighborhoods, as indicated by the median in grid cell concentrations, is similar to variability seen within some neighborhoods, as measured by the IQR. The neighborhoods with the largest $PM_{2.5}$ IQR are Bentley Island, Hamilton Acres, and Shannon Park (4.9, 6.3, and 6.5 μg m^{-3}, respectively). Every neighborhood had some grid cells with mean $PM_{2.5}$ concentrations above 20 μg m^{-3}. Parts of Bentley Island, Hamilton Acres, and Downtown West were above 30 μg m^{-3}.

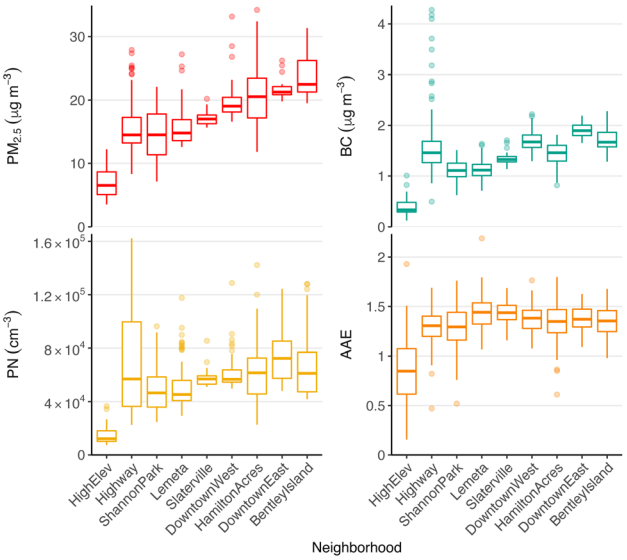

Fig. 3 Boxplots showing distribution of grid cells within each neighborhood or spatial aggregation. Neighborhoods arranged on the *x*-axis in order of increasing median $PM_{2.5}$ concentration.

Qualitatively similar results were seen for both BC and PN in the residential neighborhoods. The lowest and highest neighborhood median BC concentrations were seen in Shannon Park (1.1 μg m^{-3}) and Downtown East (1.9 μg m^{-3}), respectively. Hamilton Acres had the highest neighborhood BC IQR of 0.3 μg m^{-3}. Parts of Downtown West, Downtown East, and Bentley Island had mean BC concentrations above 2 μg m^{-3}.

All neighborhoods had median PN concentrations above 4.5 × 10^4 cm^{-3}. Downtown East had the highest median PN concentration of 7.2 × 10^4 cm^{-3}. The PN concentration across all residential areas is extremely high compared to urban mid-latitude locations. For context, in the national PN land-use regression (LUR) estimates for the continental US from Saha

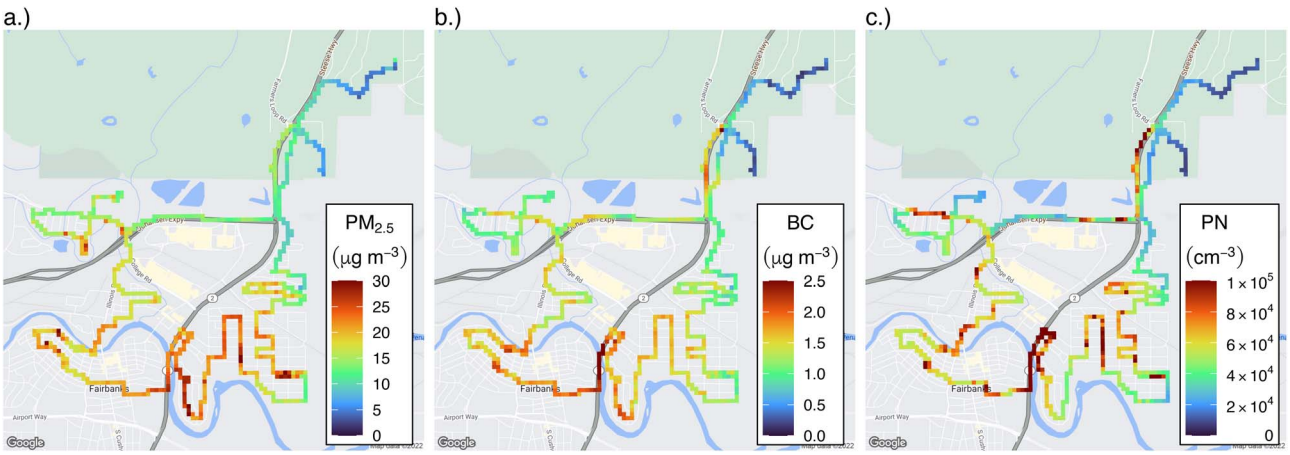

Fig. 2 Mean 50 × 50 m grid cell concentrations across all 29 drives for each of (a) $PM_{2.5}$, (b) BC, and (c) PN. All grid cells shown meet a minimum visit threshold of 10 visits.

et al.[27] the highest census block-level estimate of PN in the entire continental U.S. was 2.6 × 10^4 cm^{-3}, and typical urban PN concentrations in cities much larger than Fairbanks (*e.g.* Pittsburgh, Baltimore) were roughly 10^4 cm^{-3}. The Saha *et al.* PN estimates are annual averages, but they use a 1.1 scaling factor to seasonally-adjust for higher wintertime concentrations. Similarly, Rose *et al.*[28] present global PN measurements including from 10 urban European sites. The median wintertime PN concentration in Fairbanks is more than 4× that of the highest site from Rose *et al.*, and can be significantly higher for parts of the domain. Concurrent SMPS measurements at the ALPACA house field site suggest that the large majority of the outdoor particle number distribution (>95%) is in the ultrafine (UF, sub-100 nm) mode, though only 27% of total volume is UF (see Fig. S4†).

The distribution of AAE values across residential neighborhoods was fairly uniform. Excluding HighElev and Highway, median residential neighborhood AAE values ranged from 1.29 to 1.44, likely indicating a mix of source contribution to light absorbing PM from traffic and biomass-burning.

For each of the three pollutants, concentrations decreased dramatically at higher elevations. The HighElev spatial aggregation stands out for having considerably lower median concentrations than the residential neighborhoods or the Highway spatial aggregation, as shown in Fig. 3. Grid cells at the top of each hill were lowest even within the HighElev aggregation, as shown in Fig. 2. Median concentrations for HighElev of each of $PM_{2.5}$, BC, and PN were 6.5 μg m^{-3}, 0.3 μg m^{-3}, and 1.2 × 10^4 cm^{-3}, respectively. The least polluted part of HighElev for each of $PM_{2.5}$, BC, and PN were 3.5 μg m^{-3}, 0.1 μg m^{-3}, and 7.5 × 10^3 cm^{-3}, respectively.

Interestingly, the Highway aggregation has the lowest median grid cell $PM_{2.5}$ concentration of all neighborhoods other than HighElev, as shown in Fig. 3. Despite the low median concentration, however, it has a large number of outlier grid cells, both for $PM_{2.5}$ and especially BC. A similar pattern is seen for PN, where the median grid cell concentration is lower than other neighborhoods, but the IQR is much higher than the others. This likely reflects a higher degree of sampling near-source tailpipe emissions, which give rise to high concentrations. A full table of summary statistics for all pollutants in each neighborhood spatial aggregation is presented in the ESI (see Table S2†).

3.3 Temperature inversion impact on pollutant spatial variability

We stratify our results between two SBI categories ("strong" and "weak"), to examine how SBIs impact spatial variability for each of the three pollutants. January drives tended to have higher ΔT values than February, but there were strong and weak SBI conditions in each month. The lowest average ΔT across all drives was 0.37 °C, indicating that there was some degree of temperature inversion for the entire dataset. Fig. S2a† shows the distribution of ΔT for all drives in each of January and February.

To illustrate how the spatial variations that we see are strongly influenced by temperature inversions, we present

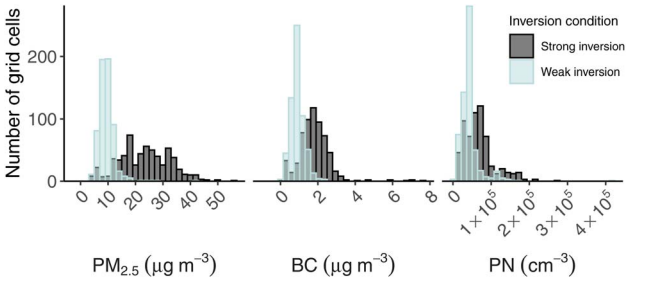

Fig. 4 $PM_{2.5}$, BC, and PN histograms of all 50 m grid cell concentrations that meet our visit threshold (visited on 10+ drives), grouped by inversion condition ("strong" or "weak").

histograms of mean grid cell concentrations of $PM_{2.5}$, PN, and BC for each inversion category in Fig. 4. All grid cells included were visited 10+ times within each inversion category. We observed higher concentrations across the large majority of the domain during strong inversion conditions for each pollutant. During strong inversion conditions, the mean $PM_{2.5}$ concentration was 23.4 μg m^{-3}, and 9% of all grid cells exceeded the EPA's 24 h fine PM standard of 35 μg m^{-3}. The 25th and 75th percentile $PM_{2.5}$ grid cell concentrations during strong inversion conditions were 16.9 μg m^{-3} and 30.6 μg m^{-3}, respectively, and the interquartile range (IQR) was 60% of the mean. During weak inversion conditions the mean $PM_{2.5}$ concentration was 9.4 μg m^{-3}, and only a single grid cell (0.2% of all grid cells) was above 35 μg m^{-3}. The 25th and 75th percentile grid cell concentrations during weak inversion conditions were 8.0 μg m^{-3} and 10.6 μg m^{-3}, respectively, and the interquartile range (IQR) was only 28% of the mean. Similar patterns were observed for PN and BC.

Fig. 5a presents a map of $PM_{2.5}$ concentration for all grid cells meeting the 10+ visit threshold for the two inversion categories. Neighborhood boxplots of grid cell concentrations for all pollutants and AAE for each inversion category are presented in Fig. 5b. We see that most of the between-neighborhood and within-neighborhood variability is seen during strong inversion conditions. During strong inversion conditions, Lemeta was the residential neighborhood with the lowest median concentration of $PM_{2.5}$ (21.1 μg m^{-3}), while Bentley Island had the highest median $PM_{2.5}$ concentration (35.5 μg m^{-3}). It is worth noting that the median of grid cell mean concentrations in Bentley Island during strong inversion conditions surpasses the EPA 24 h fine PM standard. Within-neighborhood $PM_{2.5}$ variability was high during strong inversion conditions as well. The highest within-neighborhood $PM_{2.5}$ IQR values were 9.4, 8.6, and 8.2 μg m^{-3} for the Hamilton Acres, Shannon Park, and Lemeta neighborhoods, respectively, during strong inversion conditions. Each of these neighborhoods borders open space on at least one side, and the grid cells with the lower concentrations tended to be towards these borders. Clearly neighborhood boundaries are not defined by shared air quality characteristics, but these results illustrate how air quality can be quite different even within sections of a city that nominally look and feel the same.

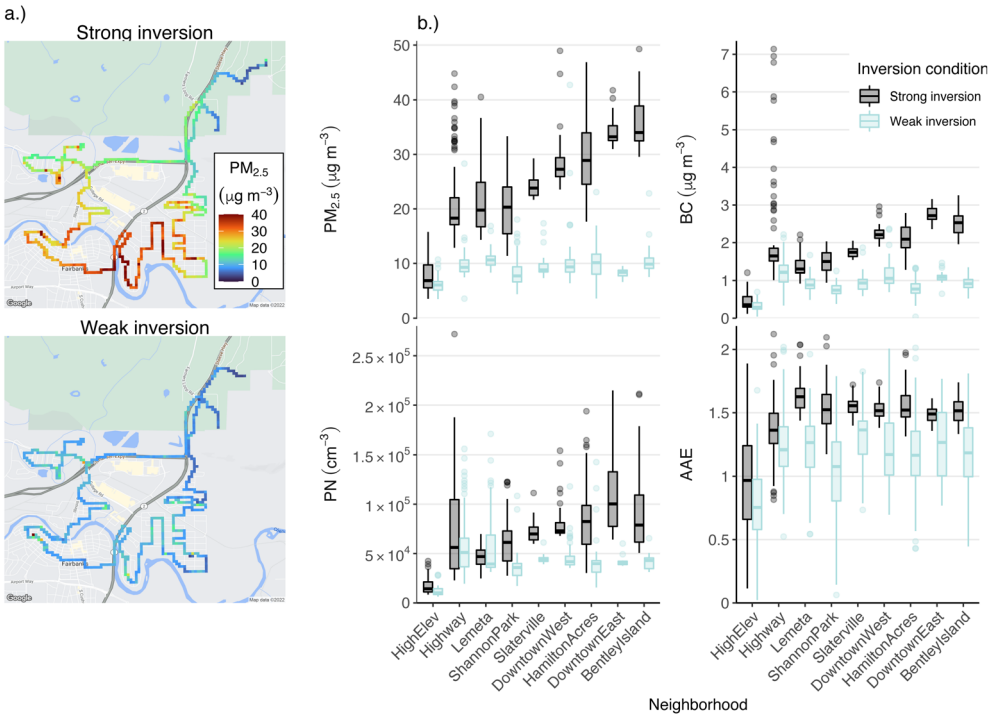

Fig. 5 (a) $PM_{2.5}$ map for strong and weak inversion conditions using 50 m grid cell aggregations. Concentration values outside of the colorscale range are given the end values of the range, for visualization purposes. (b) Neighborhood boxplots of $PM_{2.5}$, BC, PN, and AAE for both inversion conditions. Neighborhoods for all pollutants are arranged on the *x*-axis in order of increasing median $PM_{2.5}$ concentration within the strong inversion category.

Pollutant concentrations are more spatially uniform during weak inversion conditions. Median residential neighborhood $PM_{2.5}$ concentrations ranged from 7.8 μg m^{-3} in Shannon Park to 10.6 μg m^{-3} in Lemeta during weak SBI. Within-neighborhood variability was considerably decreased as well. The largest within-neighborhood $PM_{2.5}$ IQR during weak inversion conditions was 3.7 μg m^{-3}, and the average within-neighborhood IQR was 2.0 μg m^{-3}. Most of the spatial variability shown in Fig. 2 and 3 is driven by periods of strong temperature inversions, while pollutant concentration surfaces are much more flat during weak inversions. We found similar spatial patterns for BC and PN (shown in Fig. S6†).

We find a strong spatial correlation between $PM_{2.5}$ and BC grid cell concentrations (R^2 = 0.69) during strong inversion conditions, as shown in Fig. 6. BC comprises roughly 9% of $PM_{2.5}$, based on the slope of the regression line, during strong SBIs. The large majority (92%) of locations with $PM_{2.5}$ above the first concentration quartile have AAE values above 1.4. During weak inversion conditions, we see very little spatial correlation between $PM_{2.5}$ and BC (R^2 = 0.04), and there is less overall spatial variation in either pollutant. Given the lack of correlation, we do not draw any conclusions from the slope of the regression line about the BC contribution to $PM_{2.5}$. Additionally, the majority (77%) of grid cells have AAE values below 1.4,

3.4 Light absorbing PM

There is an enhancement in total light-absorbing PM across the domain during strong inversion periods, which appears to contain both BC and non-BC light absorbing material. Fig. 5b shows clearly that AAE values for all neighborhoods are higher during strong inversion periods compared to weak. For all residential neighborhoods, the median AAE values are above 1.5 and there is little spread, as indicated by the IQR, compared to weak inversions. The Highway aggregation has median AAE lower than the residential neighborhoods (AAE = 1.4), which reflects a stronger contribution from lower AAE aerosol types (such as *e.g.* pure BC) to the total light absorbing PM. High AAE values in residential areas during strong inversion periods very likely indicate a contribution of BrC to light-absorbing PM.

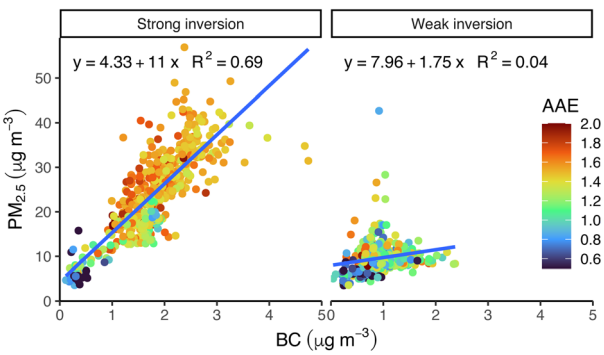

Fig. 6 Spatial correlation plots of grid cell concentrations of $PM_{2.5}$ *vs.* BC for strong and weak inversion conditions, colored by AAE.

implying that there is less of a contribution of non-BC light-absorbing material during weak inversions.

Based on the strong spatial correlation between $PM_{2.5}$ and BC during strong inversion conditions, there is likely a common source for the two pollutants. Additionally, because AAE values during strong inversion conditions are at their highest, especially where $PM_{2.5}$ concentrations are also high, it is likely that the common source driving variability is BrC-containing. And, because these high concentration and high AAE areas are largely in residential neighborhoods and not on highways, our results imply that the large majority of the spatial variability in both $PM_{2.5}$ and BC is driven by residential emissions from home-heating, as opposed to vehicle emissions. This is not to say that woodsmoke is the sole source of $PM_{2.5}$ or BC—clearly not, given some of the high BC concentration grid cells in the Highway category and lower AAE values—but that the spatial concentration gradients we observe for both pollutants are likely due to woodsmoke.

3.5 Mobile sampling results at ALPACA & ADEC stationary monitoring locations

Our mobile measurements illustrate that outdoor air at the ALPACA house field site is less impacted by particulate pollutants compared to the ALPACA downtown field site, as shown in Fig. 7. For each location in Fig. 7, we are showing pollutant concentrations measured from the mobile platform for the 50 m grid cell containing each field site or regulatory monitor. Each of $PM_{2.5}$, BC, and PN are lower for the house site compared to downtown. BC is the most dramatically different pollutant, being 1.8 times higher downtown compared to the house site. The $PM_{2.5}$ map in Fig. 5a shows that the ALPACA house sits in the midst of a strong spatial concentration gradient, where there appear to be competing influences between neighborhood wood-burning emissions and nearby open space (where emissions sources would be absent) to the immediate east of the Shannon Park neighborhood. Our sampling also shows that the downtown field site has AAE = 1.4, which is consistent with being impacted by woodsmoke during strong inversion conditions.

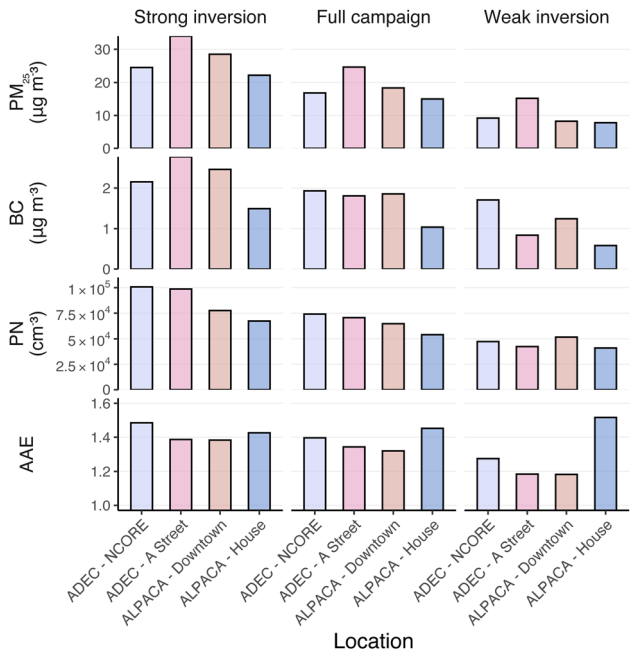

Fig. 7 Comparison of campaign-average pollutant concentrations and AAE measured by mobile sampling for grid cells containing each fixed-site location.

We also compare the aggregated mobile measurements at the locations of ADEC regulatory monitoring sites that were on our driving route. Our mobile monitoring results show that the ADEC A Street location has higher levels of $PM_{2.5}$ than the ADEC NCORE site downtown. This result is expected, given that the A Street monitoring station was sited in the Hamilton Acres neighborhood in 2019 due to concerns that the NCORE site did not capture the high $PM_{2.5}$ levels observed in residential areas. The siting of the A Street location was the result of previously conducted mobile sampling in FNSB by ADEC, which was published in the 2016 State Implementation Plan[29] and revealed the existence of large spatial $PM_{2.5}$ gradients (>10 μg m^{-3}) in different parts of FNSB during wintertime. The higher particulate pollution at A Street *vs.* NCORE that we see in our mobile measurements is consistently observed during long-term (since 2019) wintertime comparisons between the two ADEC monitors.[30]

It should be noted that the violating PM monitor in FNSB is the ADEC Hurst Road location, which is in North Pole, AK, a city 12 miles southeast of our sampling area from this study. We were not able to cover the spatial extent that would include North Pole, focusing on Downtown Fairbanks and the area around it instead. The wintertime average $PM_{2.5}$ at Hurst Road is typically roughly 2× that of the NCORE site.

3.6 Changes in pollutant concentrations with elevation

We included two steep hills in our sampling route in order to examine how pollutants are vertically stratified near the population center of Fairbanks. For both hills ("Hill #1" and "Hill #2," Fairhill Rd. and Crest Dr, respectively), we noticed stark decreases in pollutant concentrations when driving up the hill for some of our drives, and relatively no change at all for other drives. Two drives illustrating this contrasting behavior on Hill #1 are shown in Fig. 8a.

Fig. 8b shows PN concentrations from all drives on Hill #1 using boxplots for evenly spaced elevation bins, with the dataset split into the two inversion strength categories. We do not include Hill #2 for this analysis because the presence of local sources along the route (indicated by the observation of numerous plumes along the route) complicates the analysis. Elevation is in meters above valley floor, as measured from the ALPACA downtown field site, which is roughly 136 m above sea level. We performed linear regression on the un-binned data, which is also shown on Fig. 8b.

First, we see considerable variability of PN concentration within any of these elevation bins. This likely reflects temporal variation in "background" concentrations for any given day, as well as the fact that there may be some primary particle sources

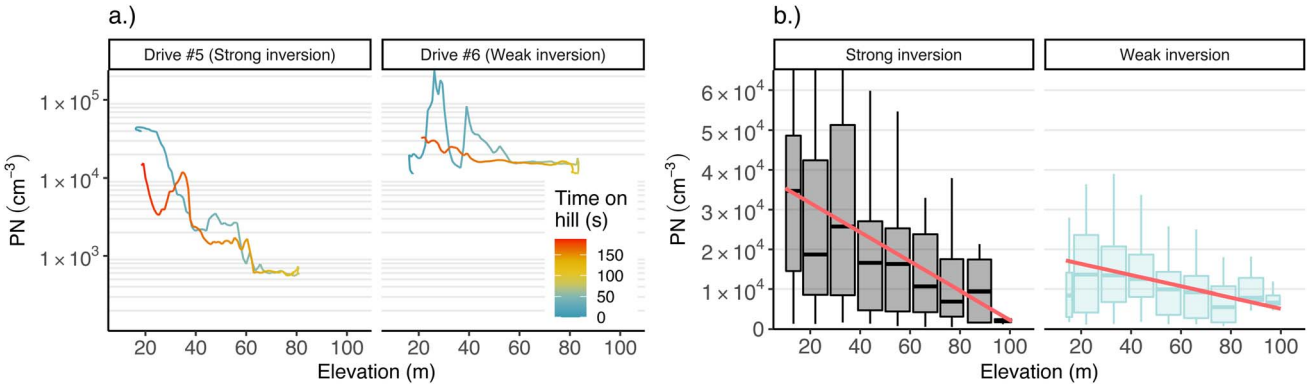

Fig. 8 (a) PN concentrations *vs.* elevation on "Hill #1" for two drives with contrasting behavior in each of the inversion categories. (b) Comparison of PN concentrations *vs.* elevation as shown by boxplots for elevation bins on "Hill #1" for all drives for each inversion category. Linear regression lines are fit to all data prior to binning.

along the Hill #1 route itself (note the large spikes in PN for "drive 6" shown in Fig. 8a). However, there are still clear differences in behavior between the two inversion categories. Bottom-of-the-hill PN concentrations during strong inversion conditions are much higher than during weak inversion conditions, consistent with the behavior observed for other pollutants discussed in the previous section. Second, the fall-off of PN concentration with increasing elevation is steeper (2.7×) during strong inversion conditions, compared to weak inversion conditions, as indicated by the slopes of the two fit lines (−368 cm^{-3} per meter *vs.* −140 cm^{-3} per meter, respectively). Lastly, the concentration at the top of the hill during the strong inversion periods is actually lower than during weak inversion periods, unlike anywhere else that we sampled. This is consistent with a lack of vertical mixing during strong inversion conditions, and increased vertical mixing during weak inversion periods. There also may be warm air advection that plays a role in diluting air at these higher elevations even while air in Fairbanks is stagnant during strong SBIs.

We see similar patterns for both $PM_{2.5}$ and BC as well. The relationship between $PM_{2.5}$ and elevation was −0.08 μg per m^3 per meter and −0.003 μg per m^3 per meter for the strong and weak inversion categories, respectively. For BC, the respective slopes were −0.01 μg per m^3 per meter and −0.005 μg per m^3 per meter, for the strong and weak inversion categories.

3.7 Co-located stationary intercomparison

The results of the instrument co-location were generally encouraging, and bolster our confidence in the accuracy of the lower-cost mobile suite used for this study. BC, PN, and $PM_{2.5}$ all had very good agreement between mobile and fixed-site instrumentation, based on the slope of a linear regression fit line (see Fig. 9). The slope of each comparison indicated agreement within 5%. The R^2 value for PN (0.97) indicates a very high degree of correlation between the MAGIC CPC and the SMPS. Similarly, the R^2 value for BC (0.82) indicated a high degree of correlation between the microAeth and the AE-33. The R^2 value for the PM comparison is substantially lower (0.62) than that of PN or BC, but still "good" in this context, given a variety of factors related to particle size and optical properties that could make the DustTrak *vs.* AMS + AE-33 comparison not apples-to-apples.

Any mobile measurement, but especially those from lower-grade sensors like the battery-powered instrument suite we

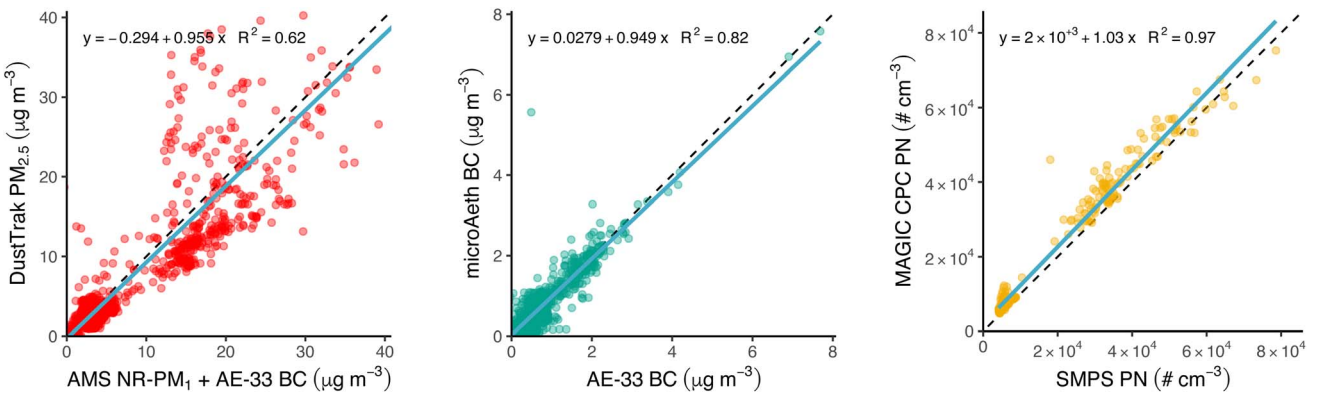

Fig. 9 Comparison of PM, BC, and PN measurements between mobile-suite instruments and stationary instruments at the ALPACA house field site during co-location.

used in this study, always require some kind of benchmarking to establish what degree of confidence the measurements reflect. Here we feel confident, based on the stationary intercomparisons, in both the absolute concentrations of each of the mobile measurements we report, and the spatial patterns of the pollutants we measured.

4 Discussion

AAE values for any light-absorbing PM are subject to a variety of influences, and so it is not a sharp tool alone for identifying biomass-burning emissions. Radiocarbon (^{14}C) or other chemical composition-based (*e.g.* mass spectrometry) source-apportionment would offer more unambiguous source determinations.[31] Nonetheless, in the context of a handful of accompanying pieces of evidence, our AAE measurements point to the major driver of spatial variability in both $PM_{2.5}$ and BC during strong inversion conditions being residential wood-burning emissions. These accompanying reasons are as follows: first, we see high concentrations of both pollutants in residential areas away from busy roads, and BC and $PM_{2.5}$ concentrations are tightly spatially correlated during strong SBIs. Second, we see elevated AAE values (>1.4) during strong SBIs in residential areas, and these AAE values are higher than what we observed on the highways. These values are consistent with what others have reported for BrC-containing PM from woodsmoke.[22,25] Third, the areas with higher concentrations of $PM_{2.5}$ also had higher AAE during strong SBIs compared to areas with lower $PM_{2.5}$ concentrations. Unequivocally, we can say that the dominant emissions sources are located in residential neighborhoods (as opposed to busy roads), that these emissions contain both BC and non-BC light absorbing material, and that, to first order given the strong spatial correlation, this emissions source drives the concentration gradients we see around downtown Fairbanks during strong SBIs. Taken together, we conclude that wood-burning is the dominant driver of spatial variability.

The tight spatial correlation between BC and $PM_{2.5}$ and the dominance of high AAE values is absent during weak inversion conditions, which indicates that woodsmoke sources cease to dominate PM during weak inversion conditions. We do not think that a shift in ambient temperature between the two inversion categories, and thus a shift in behavior regarding home heating, explains this difference. Ambient temperatures during drives in each inversion category were still quite cold in the context of home heating requirements: mean ground-level temperature for drive periods in strong and weak inversion categories were −10 and −5 °C, respectively (shown in Fig. S2b†). Thus, it is likely that the woodsmoke emissions sources remain, but the spatial PM gradients that develop around them are absent or severely reduced due to much greater dispersion, either horizontally or vertically.

It is difficult to say whether the $PM_{2.5}$ and BC hotspots we observe simply reflect the density of wood-burning stoves across neighborhoods, or are the result of a smaller subset of wood-burning sources that operate sub-optimally (the common "super-emitter" problem for primary emissions sources) and are distributed unevenly across the domain. Many others have documented that wood-burning emission factors can vary significantly by stove type,[32] operation mode,[33] fuel type and quality,[34] and time in the burn cycle,[35] among other factors. This complicates our ability to more precisely pinpoint the density and/or strength of wood-burning sources beyond our observation that the sum of the emissions impacts neighborhoods differently.

We do see evidence of traffic emissions driving spatial variability in pollutant concentrations: there are numerous outlier grid cells with high BC, $PM_{2.5}$, and PN in our Highway spatial aggregation. However, median concentrations in "Highway" are low compared to the rest of the domain. These are among the highest-volume roadways in Fairbanks (Steese Highway, Johansen Expressway), and their low concentrations relative to residential neighborhood areas imply that traffic emissions are not responsible for driving the spatial differences in PM that we observed. Taken as a whole, these data clearly illustrate that the worst of the particulate air pollution problem facing residents of Fairbanks, from a source perspective, occurs within residential neighborhoods, and thus is very likely driven by woodsmoke and exacerbated by SBI conditions. Indeed, these data are in line with ADEC's contentious, tiered "burn ban" strategy for minimizing emissions from solid-fuels burning on days where poor dispersion is anticipated. Less-polluting space-heating would considerably improve air quality in these residential neighborhoods, given the numerous emissions hot spots observed during strong inversion conditions.

The spatial gradients we observed are quite large in the context of human PM exposure. We show that, just for the neighborhoods in close proximity to downtown Fairbanks, where someone lives can greatly influence their outdoor air quality. The least-polluted parts of the domain were at the top of the two hills on our route. For example, without separating data into inversion category, top-of-hill $PM_{2.5}$ concentrations are 32 $\mu g\ m^{-3}$ lower than the most-polluted grid cell in the domain. This difference is even more dramatic during strong temperature inversions. Within the area we sampled, living near the top of one of the hills means roughly an order of magnitude lower ambient $PM_{2.5}$ exposure compared to the most polluted parts of the area. Similarly, the difference between the maximum and minimum BC grid cell concentrations is over 4 $\mu g\ m^{-3}$. Smaller, but still meaningful, exposure differences exist for residents living in different neighborhoods, or even in different parts of the same neighborhood.

Unfortunately for FNSB, the intense SBIs play a huge role in air quality for the area, and are not a modifiable factor like *e.g.* fuel choice for space-heating. Indeed, despite having stratified the drives across the two temperature inversion bins, all of our driving periods had some degree of temperature inversion. This means that cleaning up air quality in Fairbanks will always be a heavier lift compared to similar mid-latitude cities, given how magnified emissions become in a shallow boundary layer when dispersion is low. SBIs of some degree are a constant wintertime feature.

Our study also emphasizes the importance of accounting for and understanding local meteorological conditions in planning

mobile air pollution sampling and interpreting data. General oversampling is one way around this issue: with an overabundance of samples, a sampling bias across meteorological conditions likely decreases. However, in a case like Fairbanks where temperature inversions so dramatically influence pollutant concentrations, deliberately stratifying sampling across the full range of conditions is important to account for how meteorology impacts pollutant concentrations and their spatial patterns.

FNSB presents a case where accounting for spatial gradients in pollution is very important in terms of siting regulatory monitors, given the sharp gradients that exist. Because the EPA regulatory framework requires all locations within a given geographic area to be within attainment, these mobile data demonstrate how siting a monitor in *e.g.* the Bentley Island *vs.* Lemeta neighborhood would dramatically skew an air quality assessment for FNSB as a whole. Mobile monitoring like this reveals where hotspots exist, and thus where it is important to have long-term air pollution monitoring. Our mobile monitoring for the area around downtown is consistent with the long-term observed wintertime differences between the NCORE and A Street EPA monitors, and support the idea that the A Street is sited in a location where it reflects the problem of PM hotspots in the residential areas of Fairbanks. We also show that there are a handful of other locations within our small sampling domain that also reflect that problem. Similarly, we show that there are important differences in pollution levels and source impacts between the two major field sites in the ALPACA study, which are important to consider when interpreting results from *e.g.* instrument intercomparisons.

Author contributions

ESR and XT collected mobile data. MCM collected temperature data. ESR analysed data and wrote the manuscript with significant input from all other co-authors. JM and WS organized ALPACA 2022. ESR and PFD designed the study.

Conflicts of interest

There are no conflicts to declare.

Acknowledgements

Funding and support for this work comes from the U.S. National Science Foundation's Navigating the New Arctic Program under Grants NNA-90086753 and NNA-1927750, without which this study and the wider ALPACA project would not have been possible. We also owe a great debt to the on-going work done by ADEC for maintaining and operating the regulatory monitoring network in Fairbanks, which were very useful both for this manuscript and ALPACA as a whole. Special thanks to Eben Cross from Quant-AQ for facilitating the use of multiple MODULAIR-PM sensors at the ALPACA house field site and to David Warner at ADEC for helping us retrieve instruments at the Hurst Rd. site on short notice for use in this field study.

References

1 Alaska Department of Environmental Convservation, 2022, **https://dec.alaska.gov/air/anpms/communities/fbks-particulate-matter/**.
2 W. Simpson, *et al.*, *ALPACA White Paper*, 2019, **https://alpaca.community.uaf.edu/wp-content/uploads/sites/758/2019/05/ALPACA-whitepaper.pdf**.
3 L. Ye and Y. Wang, *Atmosphere*, 2020, **11**, 1203.
4 American Lung Association, *State of the Air Report*, 2021.
5 Alaska Department of Environmental Convservation, *Serious SIP Requirements, Appendix III.D.7.6 Emissions Inventory Data Amended and Adopted*, 2019.
6 T. Ward, B. Trost, J. Conner, J. Flanagan and R. K. M. Jayanty, *Aerosol Air Qual. Res.*, 2012, **12**, 536–543.
7 U.S. Department of Agriculture, *Wood Energy for Residential Heating in Alaska: Current Conditions, Attitudes, and Expected Use*, 2010.
8 Y. Wang and P. K. Hopke, *Aerosol Air Qual. Res.*, 2014, **14**, 1875–1882.
9 B. D. Busby, T. J. Ward, J. R. Turner and C. P. Palmer, *Aerosol Air Qual. Res.*, 2016, **16**, 492–503.
10 R. A. Kotchenruther, *Atmos. Environ.*, 2016, **142**, 210–219.
11 R. A. Kotchenruther, *Atmos. Environ.*, 2020, **237**, 117724.
12 J. R. Campbell, M. Battaglia, K. Dingilian, M. Cesler-Maloney, J. M. S. Clair, T. F. Hanisco, E. Robinson, P. DeCarlo, W. Simpson, A. Nenes, R. J. Weber and J. Mao, *Environ. Sci. Technol.*, 2022, **56**, 7657–7667.
13 P. L. Joyce, R. v. Glasow and W. R. Simpson, *Atmos. Chem. Phys.*, 2014, **14**, 7601–7616.
14 J. A. Mayfield and G. J. Fochesatto, *J. Appl. Meteorol. Climatol.*, 2013, **52**, 953–973.
15 M. Cesler-Maloney, W. R. Simpson, T. Miles, J. Mao, K. S. Law and T. J. Roberts, *J. Geophys. Res.: Atmos.*, 2022, **127**, 1–17.
16 H. N. Tran and N. Mölders, *Atmos. Res.*, 2011, **99**, 39–49.
17 J. Schmale, S. R. Arnold, K. S. Law, T. Thorp, S. Anenberg, W. R. Simpson, J. Mao and K. A. Pratt, *Earth's Future*, 2018, **6**, 1385–1412.
18 J. S. Apte, K. P. Messier, S. Gani, M. Brauer, T. W. Kirchstetter, M. M. Lunden, J. D. Marshall, C. J. Portier, R. C. Vermeulen and S. P. Hamburg, *Environ. Sci. Technol.*, 2017, **51**, 6999–7008.
19 D. H. Hagan and J. H. Kroll, *Atmos. Meas. Tech.*, 2020, **13**, 6343–6355.
20 S. V. Hering, S. R. Spielman and G. S. Lewis, *Aerosol Sci. Technol.*, 2014, **48**, 401–408.
21 M. S. Hammer, R. V. Martin, A. v. Donkelaar, V. Buchard, O. Torres, D. A. Ridley and R. J. D. Spurr, *Atmos. Chem. Phys.*, 2016, **16**, 2507–2523.
22 A. Helin, A. Virkkula, J. Backman, L. Pirjola, O. Sippula, P. Aakko-Saksa, S. Väätäinen, F. Mylläri, A. Järvinen, M. Bloss, M. Aurela, G. Jakobi, P. Karjalainen, R. Zimmermann, J. Jokiniemi, S. Saarikoski, J. Tissari, T. Rönkkö, J. V. Niemi and H. Timonen, *J. Geophys. Res.: Atmos.*, 2021, **126**, 1–21.

23 R. Saleh, C. J. Hennigan, G. R. McMeeking, W. K. Chuang, E. S. Robinson, H. Coe, N. M. Donahue and A. L. Robinson, *Atmos. Chem. Phys.*, 2013, **13**, 7683–7693.
24 D. A. Lack and C. D. Cappa, *Atmos. Chem. Phys.*, 2010, **10**, 4207–4220.
25 X. Zhang, M. Mao, Y. Yin and S. Tang, *Atmos. Chem. Phys.*, 2020, **20**, 9701–9711.
26 A. C. Targino, M. V. B. Oliveira and P. Krecl, *J. Hazard. Mater.*, 2022, **423**, 127133.
27 P. K. Saha, S. Hankey, J. D. Marshall, A. L. Robinson and A. A. Presto, *Environ. Sci. Technol.*, 2021, **55**, 10320–10331.
28 C. Rose, M. C. Coen, E. Andrews, Y. Lin, I. Bossert, C. L. Myhre, T. Tuch, A. Wiedensohler, M. Fiebig, P. Aalto, A. Alastuey, E. Alonso-Blanco, M. Andrade, B. Artíñano, T. Arsov, U. Baltensperger, S. Bastian, O. Bath, J. P. Beukes, B. T. Brem, N. Bukowiecki, J. A. Casquero-Vera, S. Conil, K. Eleftheriadis, O. Favez, H. Flentje, M. I. Gini, F. J. Gómez-Moreno, M. Gysel-Beer, A. G. Hallar, I. Kalapov, N. Kalivitis, A. Kasper-Giebl, M. Keywood, J. E. Kim, S.-W. Kim, A. Kristensson, M. Kulmala, H. Lihavainen, N.-H. Lin, H. Lyamani, A. Marinoni, S. M. D. Santos, O. L. Mayol-Bracero, F. Meinhardt, M. Merkel, J.-M. Metzger, N. Mihalopoulos, J. Ondracek, M. Pandolfi, N. Pérez, T. Petäjä, J.-E. Petit, D. Picard, J.-M. Pichon, V. Pont, J.-P. Putaud, F. Reisen, K. Sellegri, S. Sharma, G. Schauer, P. Sheridan, J. P. Sherman, A. Schwerin, R. Sohmer, M. Sorribas, J. Sun, P. Tulet, V. Vakkari, P. G. v. Zyl, F. Velarde, P. Villani, S. Vratolis, Z. Wagner, S.-H. Wang, K. Weinhold, R. Weller, M. Yela, V. Zdimal and P. Laj, *Atmos. Chem. Phys.*, 2021, **21**, 17185–17223.
29 Alaska Department of Environmental Convservation, *State Implementation Plan*, 2016, **https://dec.alaska.gov/air/anpms/communities/fbks-pm2-5-moderate-sip/**.
30 Alaska Department of Environmental Convservation, *Design values FNSB*, 2021, **https://dec.alaska.gov/air/air-monitoring/community-data/fnsb-summary-pm25/**.
31 S. Szidat, A. S. H. Prevot, J. Sandradewi, M. R. Alfarra, H. Synal, L. Wacker and U. Baltensperger, *Geophys. Res. Lett.*, 2007, **34**, L05820.
32 U.S. Environmental Protection Agency, *Long-Term Performance of EPA-Certified Phase 2 Woodstoves, Klamath Falls and Portland Oregon: 1998–1999*, 2000.
33 D. Bhattu, P. Zotter, J. Zhou, G. Stefenelli, F. Klein, A. Bertrand, B. Temime-Roussel, N. Marchand, J. G. Slowik, U. Baltensperger, A. S. H. Prevot, T. Nussbaumer, I. E. Haddad and J. Dommen, *Environ. Sci. Technol.*, 2019, **53**, 2209–2219.
34 A. Trubetskaya, C. Lin, J. Ovadnevaite, D. Ceburnis, C. O'Dowd, J. J. Leahy, R. F. D. Monaghan, R. Johnson, P. Layden and W. Smith, *Energy Fuels*, 2021, **35**, 4966–4978.
35 F. Fachinger, F. Drewnick, R. Giere and S. Borrmann, *Atmos. Environ.*, 2017, **158**, 216–226.